Science

# Robotics

DECEMBER 2021

AAAS

BIOMIMETICS

# Bird-inspired dynamic grasping and perching in arboreal environments

**W. R. T. Roderick[1]*, M. R. Cutkosky[1], D. Lentink[1,2]***



**Birds take off and land on a wide range of complex surfaces. In contrast, current robots are limited in their ability to dynamically grasp irregular objects. Leveraging recent findings on how birds take off, land, and grasp, we developed a biomimetic robot that can dynamically perch on complex surfaces and grasp irregular objects. To accommodate high-speed collisions, the robot's two legs passively transform impact energy into grasp force, while the underactuated grasping mechanism wraps around irregularly shaped objects in less than 50 milliseconds. To determine the range of hardware design, kinematic, behavior, and perch parameters that are sufficient for perching success, we launched the robot at tree branches. The results corroborate our mathematical model, which shows that larger isometrically scaled animals and robots must accommodate disproportionately larger angular momenta, relative to their mass, to achieve similar landing performance. We find that closed-loop balance control serves an important role in maximizing the range of parameters sufficient for perching. The performance of the robot's biomimetic features attests to the functionality of their avian counterparts, and the robot enables us to study aspects of bird legs in ways that are infeasible in vivo. Our data show that pronounced differences in modern avian toe arrangements do not yield large changes in perching performance, suggesting that arboreal perching does not represent a strong selection pressure among common bird toe topographies. These findings advance our understanding of the avian perching apparatus and highlight design concepts that enable robots to perch on natural surfaces for environmental monitoring.**

## INTRODUCTION

From perching to grasping prey, bird feet come into contact with a wide range of complex surfaces. Birds perform these behaviors frequently and with apparent ease in both urban and natural habitats. To understand how birds achieve this mechanistically, recent studies have begun to unravel the biomechanics of stereotyped takeoff and landing behaviors across a wide range of surfaces (Fig. 1A) (*1*–*4*). Studies on landing birds suggest that birds follow a time-to-contact–based guidance strategy when landing, called Tau Theory (*1*, *5*, *6*). This strategy is parameterized by τ, the time to contact at the bird's current velocity. Landing birds have been shown to maintain a constant rate of change in τ to make a controlled collision with a perch (*1*, *6*). When perching, birds pitch their body up and extend their legs and feet during the approach. After making contact with the surface, the legs absorb the bird's momentum. Meanwhile, the feet handle surface variability by wrapping and squeezing the perch with their toes. Contact is secured by combining predictable friction forces of the toe pads with stochastic forces generated by the claws, which scrape along the surface to find viable surface features to latch onto (*1*). Last, the birds balance themselves on top of the perch and adjust their footing if necessary. Internally, the grasp is actuated by muscles via tendons, and it has been hypothesized that, in many birds, specialized protruding features along a portion of the tendons running through the toes interact with accommodating features in the tendon sheaths to effectively lock the toes (*7*–*9*). In addition to perching, the legs, feet, toes, and claws of birds of prey must also grasp prey dynamically in the air. Although there are studies on how raptors pursue their prey in flight (*10*–*12*) as well as the grip forces they can produce (*13*), there are very few reports on the dynamics and behaviors associated with birds' handling contact and grasping their prey in the air. Toe topography diversity among the most common toe arrangements may represent functional tradeoffs in perching, climbing, or manipulation (*14*). However, birds with different toe arrangements occupy a myriad of ecological niches, many of which overlap, which makes it difficult to determine the relevant selection pressures.

Compared with birds, current aerial robot graspers have limited grasping capabilities. Although aerial robots have been proven useful for remote sensing, inspection, and search and rescue applications, their societal impact is held back by their limited ability to (i) grasp complex-shaped real-world objects to transport or (ii) perch and save energy. Previous grasping and perching robots were generally developed for a small range of specialized surfaces with limited demonstrated reliability (*15*). Several bird-inspired perching mechanisms did not demonstrate successful takeoff and landing (*16*–*19*). Other grasping mechanisms can pick up different stationary objects (*20*–*30*) or catch objects launched at them (*28*, *31*, *32*). Some demonstrated vertical or near-vertical landings on irregular or cylindrical surfaces (*21*, *29*, *31*, *33*–*40*), including posed branches and a single tree branch (*34*). Whereas some birds are capable of landing vertically in a slow hovering flight fashion, most of the time, they make a dynamically controlled collision. Birds also perch on a much wider range of surface geometries than current aerial robots. Further, none of these robots performs posture control to balance after perching, which is a key factor in avian perching success (*1*, *7*). Although these robots shed light on important aspects of aerial grasping and perching, none of them approaches the versatility that birds display when dynamically colliding with and reliably grasping a wide variety of complex surfaces.

[1]Department of Mechanical Engineering, Stanford University, Stanford, CA, USA. [2]Faculty of Science and Engineering, University of Groningen, Groningen, Netherlands.
*Corresponding author. Email: wrtr@stanford.edu (W.R.T.R.); d.lentink@rug.nl (D.L.)

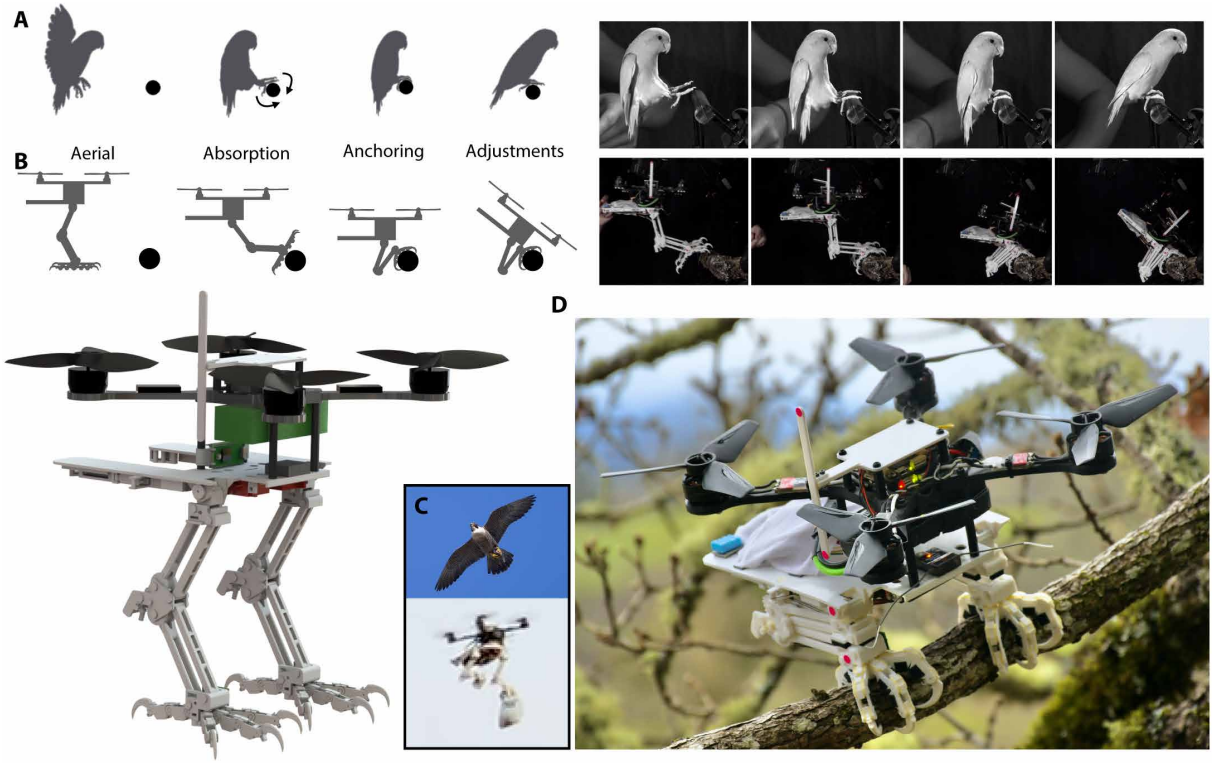


**Fig. 1. SNAG is a bird-inspired robotic leg and end effector, which enables aerial robots to take off and land on complex surfaces as well catch objects in the air.** (**A**) Birds use a stereotyped approach when landing. Upon touchdown, the bird's legs must absorb the energy of a controlled collision, which, in Tau Theory, refers to when the rate of change in $\tau$ (estimated time to collision) is greater than 0.5 (*1*, *6*). Meanwhile, their feet adapt to the surface variability of the perch to grasp it securely and to anchor the body. Last, birds adjust their footing and balance. [Bird snapshots in (*1*) have been flipped to match robot posture.] (**B**) SNAG's bipedal foot and leg system enables aerial robots to take off and land on complex natural surfaces in a controlled fashion. (Snapshots from trial #28; data file S3). (**C**) Inspired by peregrine falcons, we demonstrate that SNAG can also grasp a dynamic prey-like object in flight and carry it along (peregrine photo courtesy of George Roderick). (**D**) To illustrate its application potential in natural environments, we tested SNAG in a forest. The photo shows SNAG posed on a branch (photo edited in Apple's Photos application). For outdoor flight tests, see Fig. 8.

Leveraging our recent discoveries explaining how birds dynamically grasp a wide range of complex surfaces to perch (*1*), we developed the stereotyped nature-inspired aerial grasper (SNAG) for aerial robots (Fig. 1B). Similar to birds, SNAG harnesses stereotyped, passive, and active control behaviors across a diverse set of perches to land. SNAG integrates bird-inspired mechanisms and dimensions into its two legs that work together to grasp the perch when landing. They absorb impact energy to reconcile the momentum difference between the end effectors and the surface. During landing, SNAG also balances to stabilize itself and can safely release from the surface to take off. Experimental testing and modeling enabled us to explore the robot's perching sufficiency region: the multidimensional space of variables, including hardware design, kinematic, behavior, and perch characteristics, in which the robot succeeds at perching. Using the robot, we illustrate how the notable diversity in modern bird foot morphology is associated with modest perching performance differences across natural surfaces. Because the perch-grasping process during landing and takeoff is analogous to that of catching and releasing objects in flight, we also explored and demonstrated SNAG's ability to catch objects (Fig. 1C). Last, we show how SNAG can land on and take off from tree branches in a forest, highlighting its use as a low-cost sensor for studying natural ecosystems (Fig. 1D).

## RESULTS

### Bird-inspired grasping mechanism design

SNAG comprises a bird-inspired bipedal foot and leg system (Fig. 1). It is mounted on a quadrotor aerial platform to control its flight. The grasping mechanism structure consists of three-dimensional (3D) printed segments. Jointed subcomponents are primarily printed in place to facilitate fast iteration, assembly, and repair. SNAG can be mounted on a variety of aerial platforms. Similar to the legs and feet of birds, the grasping mechanism handles surface variability upon contact for perching robustly, enabling the aerial approach phase to be stereotyped for all surfaces during landing. Similar to some birds of prey, SNAG can also dynamically catch objects with the same legs and feet used for perching. Movie 1 demonstrates SNAG's core functionality and many of its key biomimetic design features. The first design iterations relied on more traditional engineering solutions, which underperformed. Only after 20 design iterations that increasingly mimicked bird legs and feet (see fig. S1 for the design evolution) did we reach a design that could reliably land similar to birds do (design and construction details: data files S1 and S7 and text S4).

The robot leg and grasper design are inspired by the functional anatomy of the bird hindlimb (Fig. 2, A and B). The rigid structures in bird legs and toes are made up of bone and cartilage, linked

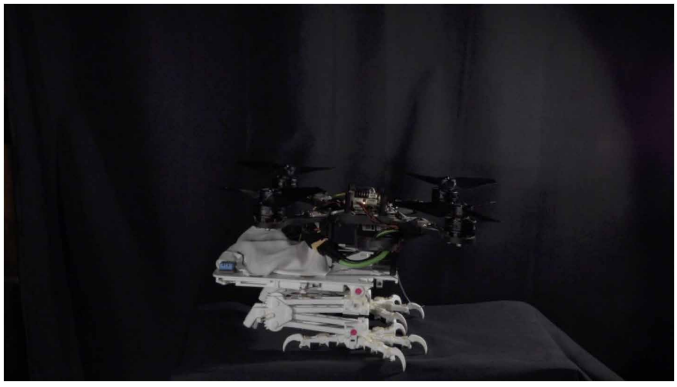

**Movie 1. Demonstration of SNAG's core functions and key design features.**

together by ligaments and actuated by muscles through tendon connections (*41*). Analogously, the robot's rigid structures are made from hard plastic, and grasping is actuated using Spectra tendons with tuned springs in series driven by one motor per leg (text S4). The dimensions of the extended leg length, toe lengths, and claw sizes were all isometrically scaled by mass from two peregrine (*Falco peregrinus*) cadavers for a ~750-g quadcopter including the mass of the SNAG grasper. We chose peregrine falcons because of their eye-catching grasp performance, which they attain with a leg length and leg mass that is typical for birds of similar body mass (text S4) (*42*). The SNAG grasping mechanism with its electronics has a mass of about 250 g. Each leg is about 50 g, or 6.7% of the mass of the quadcopter in flight. This structural leg mass is proportionally similar to that of the legs of many birds (*42*). Because birds' thighs tend to stay close to the body at all times during landing and catching (*43*), we simplified the robot leg design to resemble just the section of the bird's leg from the knee to the foot; we refer to the most proximal joint on the robot as the hip rather than the knee (Fig. 2B). The section of the grasping mechanism rigidly connected to the body holds the two actuators per leg. This design parallels how the major grasping muscles in bird legs are located more proximally than the feet (*44*). These muscles are situated above the ankle and connected to the toes via tendons (*42*, *44*). On the robot, a servomotor in the hip orients the leg in the sagittal plane at a target perch or object and also balances the robot's center of gravity during perching. The second motor stores energy in a spring, which is released upon impact with an object through a quick-release mechanism in the body (Fig. 2C). The quick release is mechanically triggered through a tendon as the leg collapses (text S4). The foot motor can reverse direction to restore and reload the leg and foot to their resting positions. The foot motor is nonbackdrivable, so it can hold grasping forces passively. The robot's legs consist of an upper and lower parallel mechanism that collapse prismatically (Fig. 2, A and B). The tendon that flexes the toes runs through the leg with a spring in series.

The robot's legs incorporate two key internal mechanisms found in many bird legs, which have been hypothesized to improve grasping performance: the digital flexor mechanism (DFM) and the tendon locking mechanism (TLM) (Fig. 2, A and D) (*7*). In the DFM, some of the tendons that flex the toes are routed around the ankle such that these tendons tension when the leg bends at the ankle. Although this mechanism has been shown to be insufficient for enabling automatic passive perching or passively curling the toes, it may still be mechanically beneficial for birds because it creates some initial stretch in the muscle, which may facilitate effective contraction (*7*, *45*). By routing the tendon around the ankle in the robot, similar to (*16*–*18*), SNAG mechanically embodies the DFM principles to (i) absorb impact energy as the collapsing leg stretches the tendon to the feet, similar to how the tendons in bird legs absorb initial impact energy (*46*), and (ii) transform the impact energy into squeeze force. Critically, passively absorbing the impact momentum with tendon-spring stretch allows the grasping mechanism to apply more grip force than the actuators could provide alone. In the TLM in birds, tendons passing through each toe interact with locking features in their associated tendon sheaths. So, when the foot actively closes, these features can lock the toe on the surface (*7*, *8*, *41*). SNAG incorporates a TLM analog with a locking ratchet in the ankle. This mechanism enables SNAG to maintain the extra grip force from the DFM when the leg collapses, preventing elastic rebound. When the foot motor resets the grasping mechanism for takeoff, the ratchet unlocks, allowing the leg to extend back into its resting position.

Similar to birds, SNAG's feet feature tendon-driven jointed toes with toe pads that generate friction and claws that latch onto surface asperities, which together enable SNAG to grasp complex surfaces reliably and securely (Fig. 2E) (*1*, *41*). The claws are 3D printed to be the same shape and size as those of an isometrically scaled peregrine falcon. Similar to bird claws, the claw geometry is sharp enough to engage with surface asperities, but not so sharp that the tip penetrates too deep into the surface and gets stuck, enabling both reliable grasping and releasing. In birds, the toe pads comprise a rough podothecal pad covering subcutaneous fatty tissue (*41*, *47*). This structure likely improves the grip; the toe pad can deform to adapt to large surface features, while the rough outer layer interlocks with the smaller surface features with relatively little tangential compliance (text S4 lists further functions). To recreate a similar toe pad structure, each phalanx in SNAG's feet contacts the surface through a deformable rubber bumper covered with a grip tape (text S4). From pilot experiments, this design remains high friction despite dirt, lichen, moss, and moisture commonly found on trees in forests, whereas smooth high-friction surfaces commonly used in robotics and engineering, such as rubber, lose grip. Overall, the hierarchical conforming structure of the jointed toes, sharp curved claws, toe pad protuberances, and rough skin complements the fractal nature of rough surfaces (Fig. 2E) (*48*). To actuate all of the toes with a single tendon from the leg, a tendon differential connects each claw to share the load equally across the toes. Similar to the mechanism birds appear to have to extend their claws (*41*), elastic bands behind the joints passively extend the toes when the foot motor relaxes the main tendon. Similar to the design of underactuated hands (*49*, *50*), it is important that the stiffness of the elastic bands is such that toes begin to curl at the more proximal joints before the distal joints when grasping an object. This allows the foot to conform well to the surface during the grasp and prevents the toes from getting stuck on surface features upon release.

The perching process commences when the hip motors rotate the legs toward the target perch and the foot motors wind up to store energy in their main springs (Fig. 2F). When the robot impacts the surface, the legs begin to collapse. The DFM absorbs the robot's flight energy and passively transforms it into grasp forces, which cause the toes to wrap the surface. Simultaneously, the quick release triggers and unleashes the stored energy to amplify the forces that flex the toes, which conform at high speed to the surface within 50 ms. As the leg collapses, the ratcheting TLM passively locks the posture

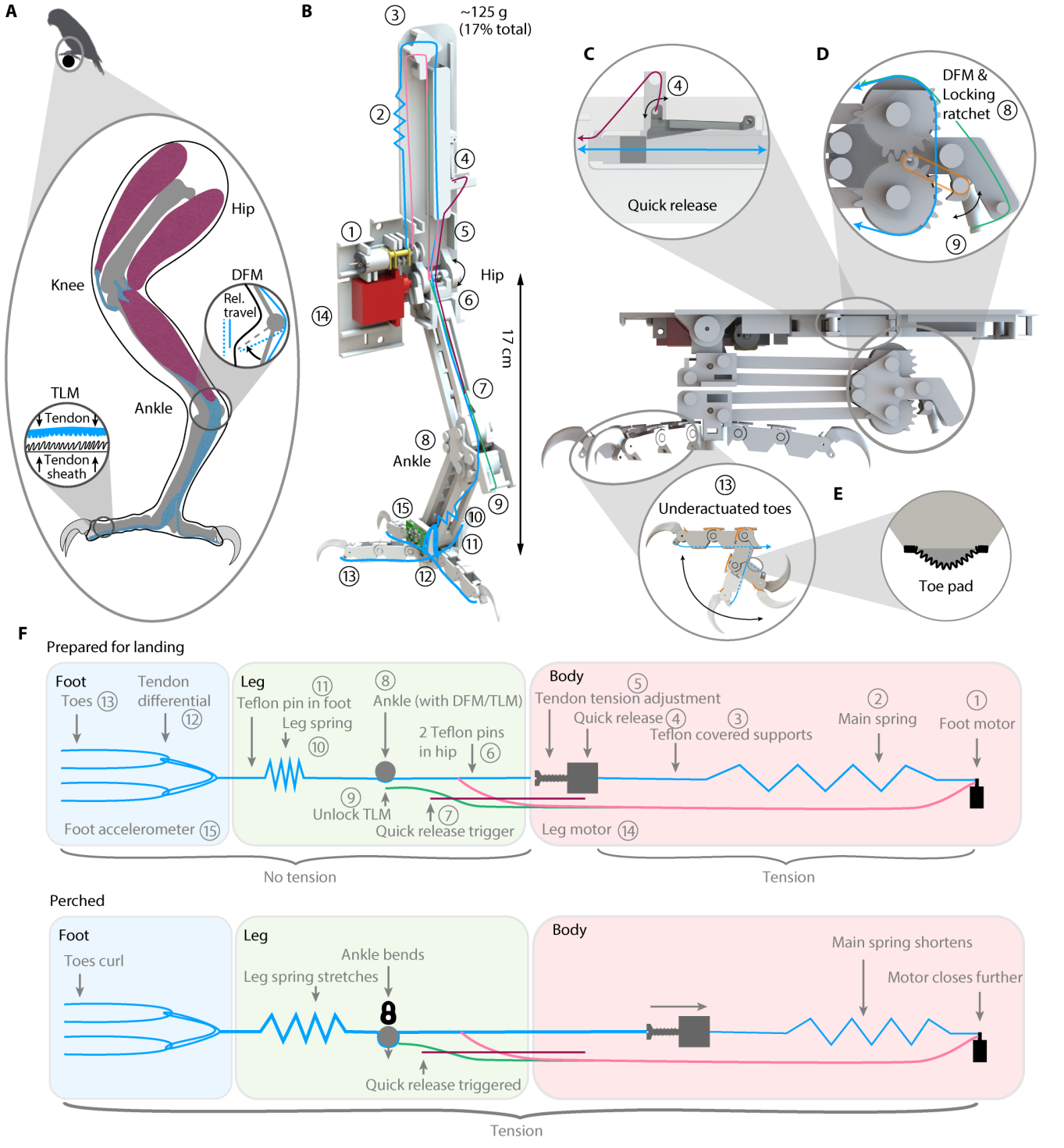


**Fig. 2. Bird-inspired grasping mechanism design.** (**A**) The robot's leg and grasper design are inspired by the functional anatomy of the avian hindlimb [drawing adapted from (*44*, *71*)]. The key dimensions are primarily scaled isometrically based off peregrine falcon legs. We integrated analogs of the avian DFM (*7*) and TLM (*7*) to improve grasping performance. (**B**) For each leg, the mechanism uses one motor for generating grasp force through a spring and another for sagittal leg motion that orients the feet at a target surface and balances the robot after perching. Triggered on impact, a quick release (**C**) releases stored energy to the tendons running along the leg, feet, and toes to the claws. Simultaneously, the grasp force is amplified by the DFM (**D**). The toes wrap around the object upon impact within 50 ms, after which the mechanism locks with the TLM. (**E**) The underactuated toes conform to complex surfaces through a tendon differential that distributes the grasping force over the toes, which each exert force on the surface via distributed toe pad friction and claws latched on asperities. For takeoff, the foot motor reverses direction to reset the entire mechanism. (**F**) The low-weight avian-inspired mechanism enables SNAG to rapidly generate high forces to dynamically grasp complex surfaces. As in birds, the most massive parts are located proximally to the body (*42*), which improves agility (data file S7). Numbered parts in (B) to (E) are defined in (F).

of the leg. During perching, an accelerometer in the right foot triggers the leg to begin balancing soon after making contact (text S4), which is accomplished through active rotation of the body about the hip. The accelerometer senses the angle of the foot relative to the direction of gravity, which we found to be a good proxy for the angle of the foot on the perch. For takeoff, initiated by the flight controller, the leg reorients to direct the quadrotor to a stable flight orientation, and the foot motor reverses direction to unlock the ankle, reset the quick release, and provide slack to the toes over about 20 s. During takeoff, SNAG relies on its rotors to propel itself away from the surface, similarly to how hummingbirds rely heavily on their wings to propel themselves from a perch (*51*).

### Grasp parameter sufficiency region

The tradeoffs birds and robots make when transitioning from the air to a perch determine the contact conditions they must handle upon touchdown (*52*). For example, landing velocities that are too high may injure the bird or damage the robot and allow less time for closed-loop feedback control. On the other hand, lower speeds result in reaching the destination later, which costs elevated slow-flight aerodynamic energy and makes the body more sensitive to approach errors induced by gusts. Landing birds and robots must balance these tradeoffs when selecting appropriate landing dynamics.

During landing, a suite of variables determines bird and robot perching success, including hardware design, kinematics, surface features, and balancing behavior after contact (Fig. 3A). Kinematic variables include the impact velocity, the angle of the body and the leg, and the angle and location at which the foot contacts the perch. Hardware parameters include dimensions and mass as well as the way the legs absorb energy. Behaviorally, after grasping a perch, birds use the feet and legs to adjust their footing and control the center of mass to balance. To accomplish this, SNAG uses an active hip joint to balance, but it cannot adjust its footing as birds do. Because these variables all interact in landing, adjustments to one can sometimes be compensated for by others to maintain sufficiency.

Ultimately, a successful landing is determined by whether the multibody dynamics, robot hardware, robot behavior, and surface conditions are suitable. The definition of a "successful landing" depends on context. For example, certain birds and bats can perch upside down, and we observed during pilot testing on small-diameter branches that SNAG can successfully stay attached to a perch by swinging underneath a branch similar to a bat. However, for our bird-inspired purposes, we define a successful landing as one in which the robot's center of mass remains above the center of the perch similar to most birds. With this definition, some amount of slip on the surface is allowable and can be beneficial for dissipating energy and stochastically finding better asperities as the claws scrape along the surface (*1*). For this definition, there are limits on the kinematic parameters that will result in a successful landing, such as bounds on the velocity magnitude and angle (Fig. 3B). Traditionally, the state-space regions that satisfy kinematic and velocity constraints for successful perching are referred to as landing envelopes (*53*–*55*). We can augment this notion of a landing envelope with all the other landing variables, including robot balancing behavior, which we term the "perching sufficiency region." Specifically, the perching sufficiency region is defined as the high-dimensional space of all of the variables that result in successful perching (Fig. 3C). This definition not only enables us to quantitatively study the effects of different kinematics and balancing behaviors when landing but also allows us to evaluate the effects of different toe arrangements across bird species. For example, different balancing algorithms or foot designs can modify the allowable velocity range on contact, shifting the perching sufficiency bounds.

Our planar perching sufficiency model defines the boundaries of the perching sufficiency region by placing limits on the linear and angular momenta, along with constraints on the foot misalignment and range of leg motion (Materials and Methods). We observed in pilot experiments that the robot's feet slipping too far forward or backward on the perch was the primary perching failure mode, which we model using angular momentum

$$\begin{aligned} H_{\mathrm{Lx}} = -v\Big(m_{\mathrm{leg}}\Big(l_{\mathrm{leg,com}} * \sin(\theta_{\mathrm{leg}} - \theta_{\mathrm{v}}) + \sin(\theta_{\mathrm{v}}) * \\ \Big(-\frac{d}{2} * \cos(\theta_{\mathrm{leg}})\Big) + \cos(\theta_{\mathrm{v}}) * \Big(\frac{d}{2} * \sin(\theta_{\mathrm{leg}})\Big)\Big) - \\ m_{\mathrm{body}}\Big(l_{\mathrm{body}} * \sin(\theta_{\mathrm{leg}} - \theta_{\mathrm{v}} - \theta_{\mathrm{bal}}) - \\ l_{\mathrm{leg,eq}} * \sin(\theta_{\mathrm{leg}} - \theta_{\mathrm{v}}) - \sin(\theta_{\mathrm{v}}) * \Big(-\frac{d}{2} * \cos(\theta_{\mathrm{leg}})\Big) + \\ \cos(\theta_{\mathrm{v}}) * \Big(\frac{d}{2} * \sin(\theta_{\mathrm{leg}})\Big)\Big)\Big) \end{aligned} \tag{1}$$

where the variables are as follows: $v$, speed; $m_{\mathrm{body}}$, body mass; $m_{\mathrm{leg}}$, leg mass; $\theta_{\mathrm{leg}}$, angle of the leg; $\theta_{\mathrm{v}}$, angle of the velocity; $d$, perch diameter; $l_{\mathrm{body}}$, body length; $\theta_{\mathrm{bal}}$, balance angle; $l_{\mathrm{leg,\,eq}}$, extended leg length; and $l_{\mathrm{leg,\,com}}$, projected location of the center of mass on the axis of the legs (Fig. 3A, Materials and Methods, and data files S2 and S4). We estimate the limits on the angular momentum upon contact with the perch, $H_{\mathrm{Lx}}$, by corroborating this mathematical model (Fig. 3A) with our experimental perching data (Figs. 4 to 6). The model's other four constraints beyond surface slip ensure that the robot collides with enough momentum to collapse the leg, the robot collides softly enough to avoid damage, the foot is reasonably aligned with the perch to ensure a good grasp, and the robot has enough balance angle range before hitting the angle limit to balance effectively. We use 2D slices from this model to visually illustrate how the variables interact in determining perching sufficiency. The simplicity of the model allows us to gain critical intuition into the key considerations that govern perching.

### Experimental investigation of the perching sufficiency region

To study SNAG's perching performance and corroborate how the kinematic, hardware, behavior, and perch parameters drive its perching sufficiency parameter region, we set up a series of controlled perching experiments (Fig. 4A and Materials and Methods). The experimental setup precisely launched the robot by pulling it along a rail with an elastic band, until it was released into the air immediately before its foot impacted the surface, which triggered SNAG to grasp the perch. For these tests, the robot did not use its rotors because the rail system allowed for high precision in specifying and varying the kinematics at contact. We focused on how foot morphology, balancing strategy, landing velocity, impact angle, leg angle, and surface properties affect perching across branches of different sizes and textures (table S1). For these tests, we selected impact conditions in the realm of what birds experience by focusing on tree branches to perch and a range of objects of similar mass as prey to catch (Materials and Methods and text S5). During the experiments,

about 190 trials in total, the robot configurations performed highly reliably and experienced little wear (data file S3), justifying our mathematical model assumptions. Movie 2 illustrates the range of experiments and highlights the similarity in landing behavior to birds that we reported earlier (*1*).

Across the class Aves, there exist many different toe arrangements, frequently associated with lifestyle and ecological niche (*56*, *57*). The two most common toe arrangements are anisodactyl [three toes in the front and one toe in the back, found in peregrine falcons among other groups (*56*)] and zygodactyl [two toes in the front and two toes in the back, found in parrotlets among other groups (*58*)] (Fig. 4B). Both toe topographies have opposable toes, and both enable birds to perch. However, to our knowledge, there have been no experimental studies into how these toe arrangements affect perching or grasping performance in birds (*59*).

To experimentally compare the perching performance of the two toe arrangements, we analyzed SNAG landing at different speeds with anisodactyl and zygodactyl foot designs (Fig. 4, B and C, and text S4). Our hypothesis was that more toes on one side will help with handling angular momentum in the opposite direction (rationale in data file 14). Thus, we would expect that the thresholds on the landing speed limits would be lower for the anisodactyl feet as compared with those of the zygodactyl feet. We tested the robot on two sections of an Oregon white oak (*Quercus garryana*) branch (64 mm in diameter). For the purposes of these tests only, we counted the landing as a success if the robot was able to bring the robot to rest (in two landings that we counted as successes, the robot fell off

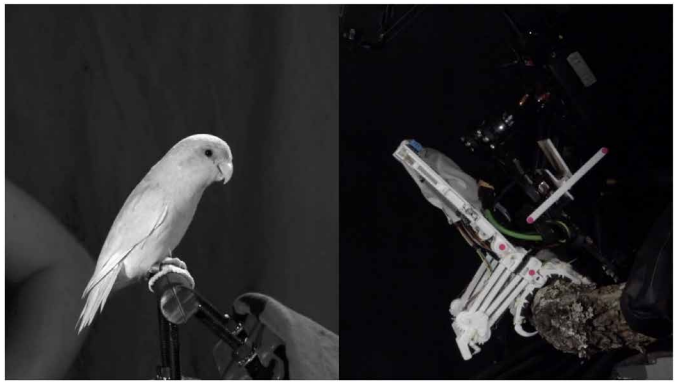

**Movie 2. Bird-inspired dynamic grasping and perching in forest environments. All robot clips are slowed four times unless otherwise marked.** All parrotlet clips are slowed 12.5 times and flipped horizontally. The speed difference may be explained by the mass difference between the parrotlet [~30 g; video in (*1*)] and robot (~750 g).

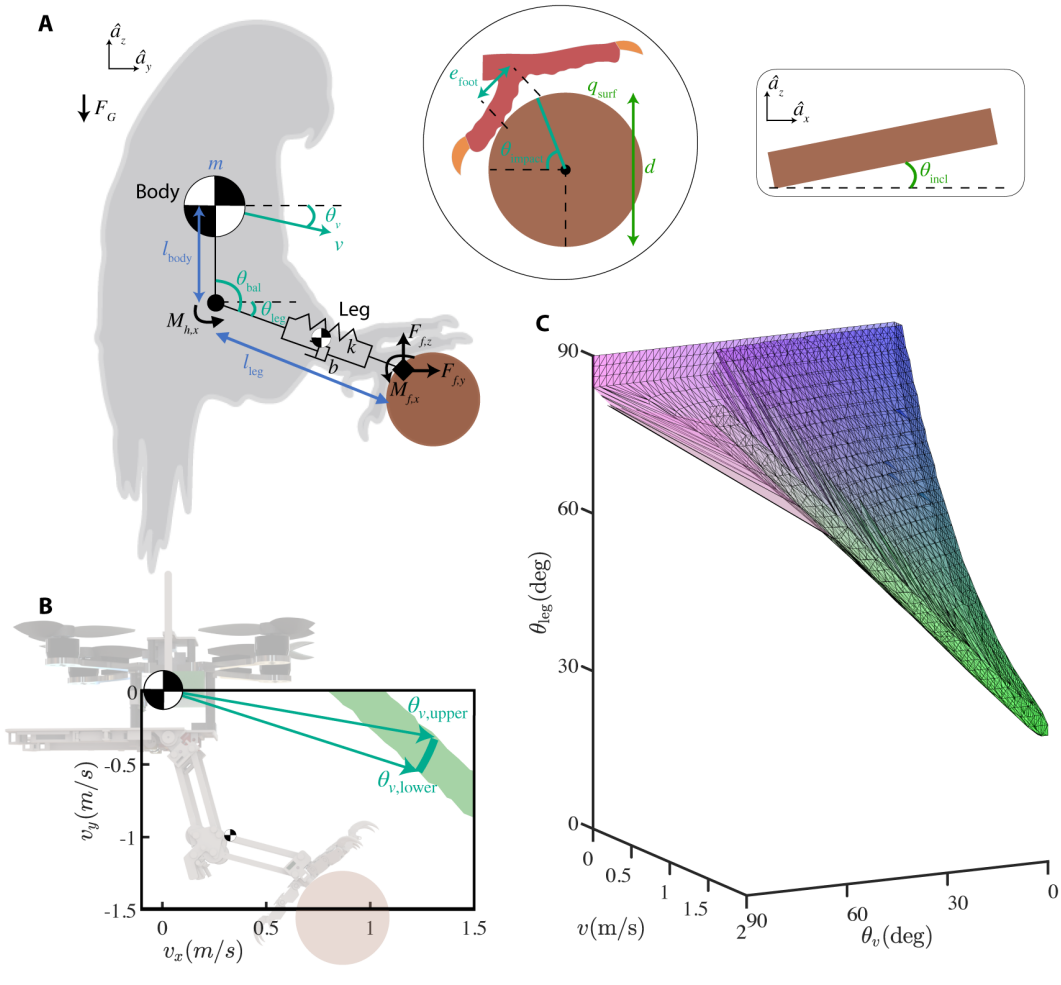


**Fig. 3. The grasp parameter sufficiency region for perching.** (**A**) Perching success is determined by leg and foot design, kinematics, surface features, and balancing behavior after contact. (**B**) All variable combinations that meet the requirements to grasp and hold onto the surface for the impact condition fall into the sufficiency region. For each variable, holding all others constant, there is an upper and lower bound. As an example, the curve within the green region indicates the upper and lower bound for the impact velocity angle. The drivers behind these bounds include the dynamics, surface friction, leg motor torque, and leg spring and structure stiffness. Much of the energy in the direction of the vector from the hip to the feet will be absorbed by the springs in the legs. The energy perpendicular to that vector will be, in part, absorbed in rotating the center of mass of the robot, raising the height of the center of mass, system compliance, slipping on the surface, and play in the mechanism. (**C**) Our multiparameter model predicts the perching sufficiency range in parametric space. The 3D sufficiency subspace illustrating the approach speed ($v$), the approach angle ($\theta_v$), and the leg extension angle ($\theta_{leg}$) shows how they are required to interact to result in perching success. The colors were selected for visualization purposes: The amount of red, green, and blue in each face corresponds to the degree of velocity angle, velocity magnitude, and leg angle, respectively, relative to their extremes.

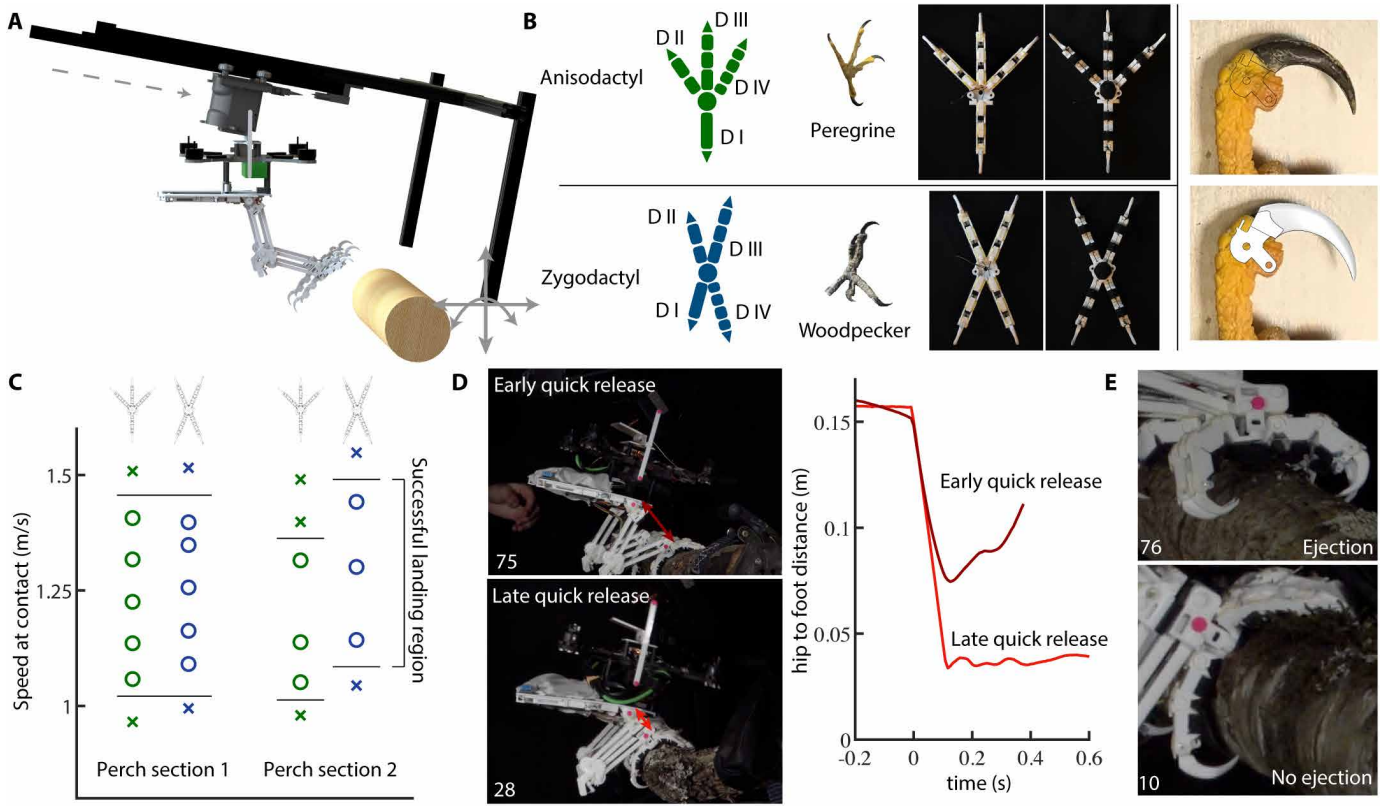


**Fig. 4. Experimental investigation of perching sufficiency: The effect of toe arrangement, quick-release trigger timing, and foot ejection.** (**A**) To study SNAG's grasp sufficiency region and to understand the roles of the hardware, kinematic, behavior, and perch parameters, we set up a series of controlled collisions with tree branches in which we varied the impact and surface conditions. The robot is attached to an elastic band-driven rail system that launches it into the air immediately before impact with the perch. (**B**) To test how perching success depends on bird foot morphology, we tested the two most common toe arrangements: anisodactyl, three toes in the front and one toe in the back (e.g., parrotlets and woodpeckers), and zygodactyl, two toes in the front and two toes in the back (e.g., peregrine falcons). (Background of the bird foot images was removed for clarity.) (**C**) To determine whether more toes on one side helps the robot absorb angular momentum in the opposite direction, we tested both toe arrangements at different perching impact speeds and, thus, proportionally larger angular momentum (Fig. 3A). The nominal velocity angle at impact was kept constant and representative for bird landing, 10°. We observed no difference on the first section of a natural perch, a tree branch, and we observed a small shift in successful perching speeds on the second perch section. Open circles indicate perching success, whereas crosses indicate failure. The min/max differences for the upper and lower thresholds on the second perch section are 0.04/0.23 m/s and 0/0.16 m/s, respectively. (**D**) A key hardware design parameter that influences the grasp sufficiency region is the timing of the quick-release trigger. If the trigger is too early, then the leg becomes too stiff to collapse, resulting in a failed landing. However, a late trigger can cause less energy to be absorbed by the legs, which increases the likelihood of damage to the robot. (**E**) Last, improper foot and leg hardware design (such as claw forces or rebound forces that are too high) can also cause the foot to eject from the surface. (Numbers in the bottom-left corner indicate the trial number; data file S3.)

the perch because the balance behavior was too vigorous; data files S3 and S4). We found no difference in the thresholds on one perch section and a slight offset in the thresholds on the other (Fig. 4B). Although the offset on the second perch section corresponds to our hypothesis, the largest difference in thresholds is too small to be confident that there is consistent functional relevance for perching birds and robots (min/max differences: 0.04/0.23 $ms^{-1}$ upper bound and 0.00/0.16 $ms^{-1}$ lower bound).

Hardware design determines how the robot absorbs impact energy and whether the grasp will eject (text S9). For example, if the tension in the tendon of the leg is too high, then the legs will not fully collapse (Fig. 4D). However, if the tension is too low, then little flight energy is absorbed when the leg fully collapses; as a result, the robot collides with the surface at a higher speed, which could cause additional wear and damage over time. In addition, improper leg and foot design can lead to ejection, which we observed in some of our earlier SNAG prototypes (Fig. 4E). Upon close examination, we found that ejection can also occur in birds when they curl their claws to grasp slippery surfaces, such as Teflon (movie S1) (*1*). With a combination of design updates, including changing the balance of forces curling the toes, hard stops on the claw curling angle, and reducing the rebound after impact, the final SNAG design avoids this problem.

We found that active balancing behavior markedly improves perching success by widening the perching sufficiency region. To experimentally assess the effects of different balance strategies on the perching sufficiency region, we tested the robot landing with fixed leg angle, open-loop, and closed-loop algorithms (Fig. 5, A and B; fig. S2; and text S7 for balance model). The fixed leg angle algorithm entails commanding a constant balance angle to the leg, which requires the foot to hold relatively large pitch-back moments for a successful landing. There is some small variation in the leg angle

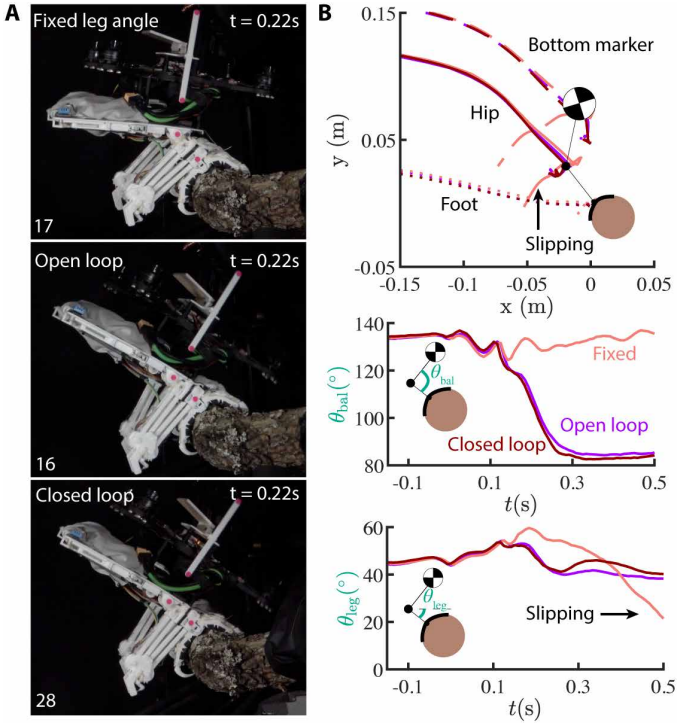


**Fig. 5. Experimental investigation of perching sufficiency: The effect of balance behavior after contact.** (**A**) We experimentally verified the perching stability that three different balance algorithms afford: The first control scheme maintains a fixed leg angle, the second is open loop, and the third is closed loop (control loop details are in Materials and Methods). The fixed leg angle scheme commands a relatively high balance angle during landing, whereas the open-loop and closed-loop algorithms rotate the body forward, which much reduces the balance angle. (**B**) For the same conditions, the fixed leg angle resulted in a failed landing, whereas the open-loop and closed-loop algorithms resulted in a successful landing because the robot was able to place its center of gravity near the top of the perch. The white bar with pink dots on the robot body enables kinematic tracking and serves as a scale bar.

with this algorithm due to finite motor forces, mechanism compliance, and nonzero tolerances. The closed-loop algorithm functions as follows: After a delay (while the leg collapses), the robot commands its center of mass to move toward the top of the perch using feedback from the accelerometer on its right foot (text S4). The open-loop behavior functions similar to the closed-loop algorithm, but with one modification; the algorithm commands a constant balance angle, equivalent to what would be expected in the closed-loop case if the foot maintained the same orientation as when it made contact with the perch. We found that, when SNAG used the fixed leg algorithm, the robot was not able to successfully perch with the control impact conditions (in two different landing conditions), and it fell backward after absorbing the impact energy (data file S3, trials #17 and #65). On the other hand, we would expect that the open-loop control would perform as well as the closed-loop control, so long as the foot does not slip substantially. SNAG succeeded at perching under both the open-loop and closed-loop algorithms with nearly identical kinematics. However, we did record one open-loop control trial in which the robot failed to land; although that may be due to an error found in the code that was corrected for the successful open-loop landing, the kinematics appeared similar in both cases (data files S3 and S4). When landing vertically with appropriate contact conditions, the robot was able to land successfully with both the fixed and closed-loop algorithms (Fig. 6B).

Focusing on the peregrine falcon anisodactyl toe arrangement and closed-loop balance control for the rest of the experiments, we study the effects of leg orientation and foot placement on the perching sufficiency region (text S8). At first foot-surface contact, there are three primary parameters that influence perching performance: the leg angle ($\theta_{leg}$), the impact angle ($\theta_{impact}$), and foot misalignment ($e_{foot}$) (Fig. 3A). If the foot misalignment is too high, then the toes will curl too far before contacting the perch, resulting in a failed landing (Fig. 6A). Higher leg and impact angles will result in more angular momentum over the center of the perch. If the angular momentum is too high, then the robot fails to land successfully and violates the upper angular momentum constraint in our model (Fig. 6A).

Both the magnitude and the direction of the robot's velocity on contact shape the perching sufficiency region (Fig. 6B). If the robot approaches the perch at shallow velocity angles, then the robot violates the angular momentum constraints of the sufficiency region model and fails to land experimentally when the impact speed is too high or too low. Too low a speed may also cause the legs to not collapse fully, which increases the pitch-back moment and can result in failure. To account for this effect, our model places a lower bound on the acceptable linear momentum. On the other hand, if the robot drops vertically onto the perch, then gravity is sufficient to collapse the leg fully even at an initial velocity of 0 m/s. In this case, the robot gains speed as the leg collapses. If the robot lands too hard on the perch, however, then components can break. Therefore, our model also incorporates an upper bound on the linear momentum, which we did not probe experimentally.

In addition to kinematic, hardware, and behavior tradeoffs, the properties of the perch itself can change the size of the perching sufficiency region (Fig. 6C). We tested three diameters of an oak tree: 38 mm (1.5 inches), where the feet can wrap around most of the perch; 64 mm (2.5 inches), where the feet wrap about halfway around the perch; and 165 mm (6.5 inches), where the feet wrap less than a quarter of the way around the perch. Parrotlets can accommodate perches of similar proportions relative to their feet (*1*). SNAG can land on each diameter. On small-diameter perches, SNAG's feet can fully wrap the surface, causing more tendon length to be drawn from the feet. Consequently, leg stiffness and grip force are reduced. On the other hand, larger diameter perches, which tend to have larger asperities, prevent the foot from closing. This amplifies the leg stiffness and the grip force. We also tested a medium diameter alder tree (*Alnus*) with relatively smooth bark and some moss on top. Smoother bark makes the claws more likely to eject the foot, but we found that SNAG successfully lands on this slippery perch. Further, although many tree branches are nearly horizontal in nature, there are also many that are angled in a vertical plane. Our experiments demonstrate how the independent passive energy absorption from each leg enables SNAG to accommodate these angular variations (Fig. 6D). However, a small amount of foot misalignment can cause the robot to fall (data files S3 and S4).

Last, SNAG is able to catch a wide variety of objects harnessing the same hardware as for perching (Fig. 7). Catching is, in many ways, analogous to perching. The main differences are the velocity of the grasper and the object, the textures of the object, and the forces imparted on the grasper (text S3). Our laboratory experiments show

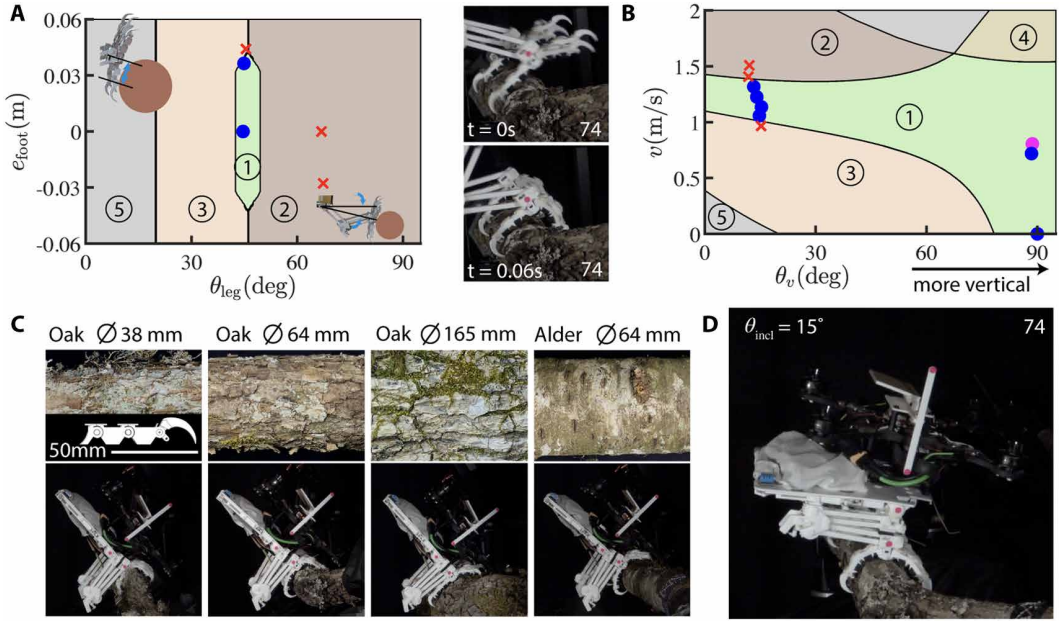


**Fig. 6. Experimental investigation of perching sufficiency: The effect of leg orientation, foot placement, impact velocity, and surface conditions.** The perching sufficiency space is divided into the following five regions: 1, success (green); 2, angular-momentum upper-bound constraint violated (dark brown); 3, angular-momentum lower-bound constraint violated (light brown); 4, linear-momentum upper-bound constraint violated (dark yellow); 5, two or more constraints violated (gray). A description of the model can be found in Materials and Methods. (**A**) A 2D slice of the perching sufficiency region shows how foot misalignment versus leg angle affects the robot's ability to perch. Perching fails when the magnitude of the foot misalignment is too large (red cross that borders regions 2 and 3) and when leg angles become too large, breaking the body angular-momentum upper-bound constraint (red crosses near the middle of region 2). The blue dots indicate successful landing experiments, and the red crosses indicate failed trials. The photos illustrate how foot misalignment causes the toes to curl before contacting the surface. (**B**) The robot faces both linear and angular momentum constraints, illustrated by a 2D slice of perching sufficiency plotted as a function of velocity magnitude (speed) versus velocity angle. To distinguish the linear and angular momentum constraints, we linearly interpolate the leg angle based on the velocity angle, using 10°/45° and 90°/0° ($\theta_v/\theta_{leg}$) as end points. Because there are small kinematic variations from trial to trial, we also ran the model with the specific kinematics of each trial, and the successes and failures agreed in all cases. The magenta dots correspond to using the fixed leg algorithm as opposed to the closed-loop algorithm in blue and red. There is an obscured magenta dot under the blue dot at (90,0). (**C**) Branch diameter and surface friction also influence perching performance. SNAG successfully lands on all four surfaces tested: a small (38 mm)–, medium (64 mm)–, and large (165 mm)–diameter perch of the same oak tree species as well as a 64-mm-diameter alder tree perch (text S5). (**D**) Many branches in nature have an inclination (are angled in a vertical plane), which SNAG can accommodate with its independent passive energy absorption in both legs. The demonstration here shows a vertical landing on a branch at a moderate inclination angle.

that SNAG can catch and release objects of similar size and weight to the prey of peregrine falcons (*60*) using peregrine falcon–inspired feet (Fig. 7, Materials and Methods, and data files S3 and S4). We also found that SNAG is able to catch objects during outdoor flight (Fig. 1D).

### Application potential in forest environments

To demonstrate how SNAG can be used to enable quadcopters to monitor the natural environment at low energetic cost, we tested its perching performance in a forest (Fig. 8, A to C). For these tests, the robot was manually flown by the pilot with a remote controller (RC) (Materials and Methods). We dynamically perched SNAG on the surface of a Douglas fir (*Pseudotsuga menziesii*) during a bird-inspired near-horizontal landing (Fig. 8A). Despite high foot error causing the front toes to curl prematurely, the robot perches successfully, demonstrating its robust bird-like performance. Tests with a vertical approach show that it can take off from the ground, land on a tree surface, rest perched on the surface, and take off to return (Fig. 8B). While perched, SNAG can characterize the microclimate by recording temperature and humidity for environmental research (Fig. 8, A to D; data reported in data file S4).

## DISCUSSION

Inspired by how birds land on perches, we developed SNAG. The dynamic perching performance of SNAG shows how a stereotyped set of bird-inspired behaviors and mechanisms for landing is sufficient for perching robustly: The legs orient toward the perch during the approach; upon impact, the collapsing legs absorb energy and passively amplify the grasping forces via a tendon differential to the feet; simultaneously, the toes conform to the surface and generate reliable friction with toe pads and stochastic forces with claws latching onto surface asperities; when the legs have fully collapsed, SNAG locks in place automatically; and SNAG balances its center of gravity over the perch. This enables SNAG to grasp beforehand unknown complex surface geometries and textures, such as branches covered with dirt, lichen, moss, and moisture, commonly found on trees in forests. SNAG's robust leg and feet performance is accomplished within the same weight budget allocated in birds, 6.7% body weight (*42*), and each of SNAG's legs can hold 10 times its own weight (text S4).

We found that the robotic embodiment of key internal mechanisms in bird legs (Fig. 2) enables SNAG to grasp natural surfaces with high passively maintained forces at high speed, within 50 ms. First, upon impact, the avian-inspired DFM transforms impact energy into grasp forces due to the routing (and stretching) of the elastic leg tendon. In parallel, the leg collapse mechanically triggers a quick release to contribute additional tendon force. Our experiments show the importance of when the trigger occurs after impact. Too early makes the leg too stiff to fully collapse, while too late reduces the energy absorbed and thus increases the likelihood of damage (Fig. 4D). These experiments suggest that the timing of leg muscle and tendon tension onset may be equally important in birds and other animals. As the legs collapse, the avian-inspired TLM acts

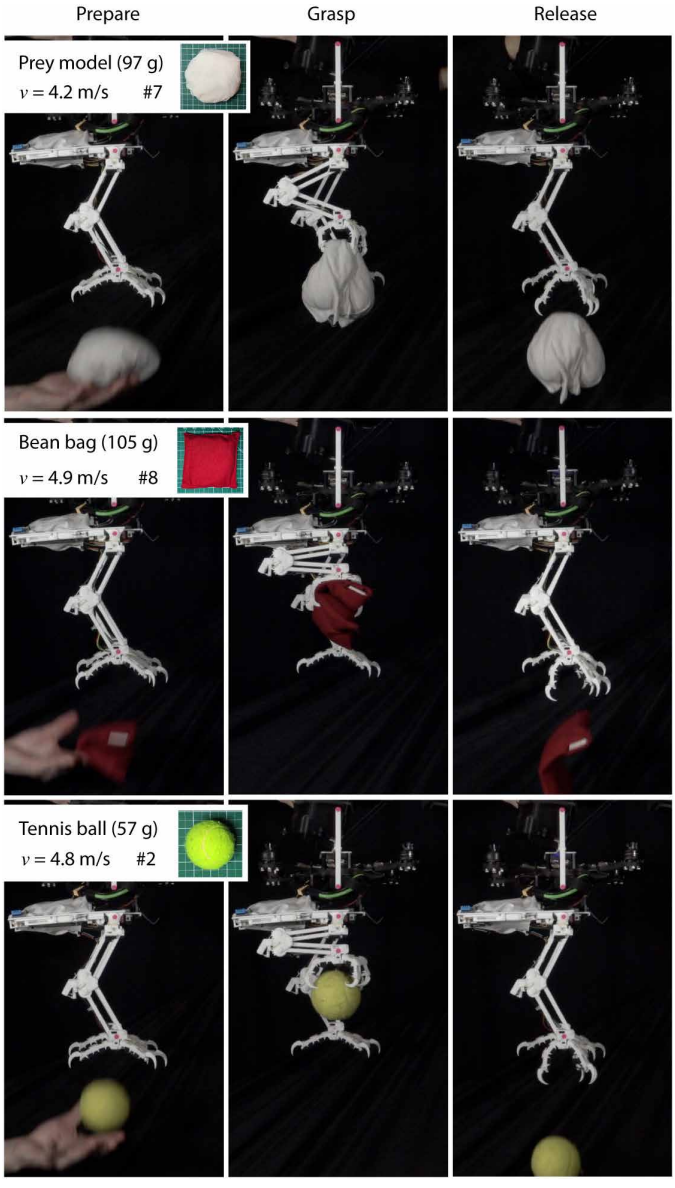


**Fig. 7. Experimental investigation of SNAG's catching ability.** We found that SNAG can successfully use the same anisodactyl peregrine falcon–inspired grasper hardware for dynamic perching and catching, despite being optimized for perching. This mirrors how peregrine falcons can use their legs and feet to both perch and catch prey. The video frames illustrate how SNAG successfully catches objects tossed into its feet, stably holds on to them, and releases them in a controlled fashion when triggered. The velocity difference between the feet and object is about 5 m/s, which is small to moderate compared with the dynamic catching behavior of most birds of prey. All three objects—a prey model, the bean bag, and the tennis ball—have a similar size and weight as peregrine falcon prey (*60*).

as a ratchet to lock the leg and maintains grasping forces passively. Grasp forces are distributed equally over all toes via the tendon differential that connects the leg tendon to each toes' claw. The speed of the grasp is partly due to the small size and weight of the grasper (data file S7), facilitated by moving the actuator and mechanism weight proximally, as in birds (*42*). To reliably exert grasping forces on irregular geometries and textures similar to birds, SNAG embodies feet with jointed toes, compliant toe pad protuberances with rough skin and sharp curved claws that conform to hierarchical textured surfaces (*48*). As in birds, SNAG's claw geometry is sharp enough to engage with surface asperities, but not too sharp; the claws can deform compliant surfaces without penetrating them to the point of getting stuck, to ensure they release reliably. To release its grasp, SNAG harnesses avian-inspired (*41*) elastic bands behind the toe's joints to passively extend the toes and claws when the foot motor relaxes the leg tendon.

For each leg, SNAG's 14 degrees of freedom are controlled by just two motors based on sparse information. The hip servomotor orients the leg right before perching and balances the robot after landing by rotating the center of mass toward the center of the perch similar to a bird (Fig. 4). The active balancing is informed by an accelerometer that senses the impact and the direction of gravity in the right foot relative to the foot itself, which is a good proxy for the angle of the foot on the perch. The foot motor stores energy for tensioning the leg tendon before perching and releases tension before takeoff. This motor also actuates all of the toes of the foot, controls the leg stiffness, and unlocks the TLM before takeoff. So rather than controlling every degree of freedom independently as in classic walking robots such as ASIMO (*61*), SNAG underactuates its two robotic legs and feet similar to passive dynamic walkers with a few actuators and sensors (*62*). The passive dynamics drive the underactuated adaptation to surface features upon contact when feedback loops are too slow or incomplete, serving a similar role to the open-loop and feed-forward control in many animals (*63*). For example, higher impact speeds collapse the leg more quickly, which causes the toes to wrap an object more quickly. As a result, the timing of the grasp passively adjusts to the timing required for handling the impact speed. However, whereas birds can situate their center of mass (*4*), using feedback from their visual, tactile, and vestibular systems as well as their lumbosacral organ (*64*, *65*), SNAG only has access to the direction of gravity through the accelerometer in its foot. SNAG's ability to balance, even if rudimentary, suggests that animals may only need sparse knowledge of their state and the environment to successfully perch and balance. Further, the similarity in perching performance with the open-loop and closed-loop control suggests that balance behavior itself can be largely stereotyped in the absence of large slip. Sensor fusion of the exceptional avian sensor suite can then serve to make their perching performance particularly robust in complex environments, a strategy that may serve future robots. Furthermore, birds often use their wings and tail to help them balance in addition to their legs (*4*), although we observed in previous work that perching parrotlets sometimes close their wings on landing (*1*). SNAG's landing and balancing without aerodynamic support confirms that this is sufficient; however, future designs (data file S8) may balance even better by generating aerodynamic forces that grow the sufficiency region similar to birds.

The notion of the sufficiency region itself offers a paradigm for robot design and control. As robots such as SNAG move out of the laboratory into unstructured environments, optimizing for classic parameters, such as the total finger force (*66*), is only valuable in so far as they improve the likelihood of achieving the robot's goal. In many cases, a robot's goal is to complete a task consistently and sufficiently quickly rather than to achieve an optimal proxy metric. Thus, future robots will need a paradigm shift from the common approaches in robotic grasping of variable surfaces that are relatively slow and require high-quality sensory information (*67*); for robots

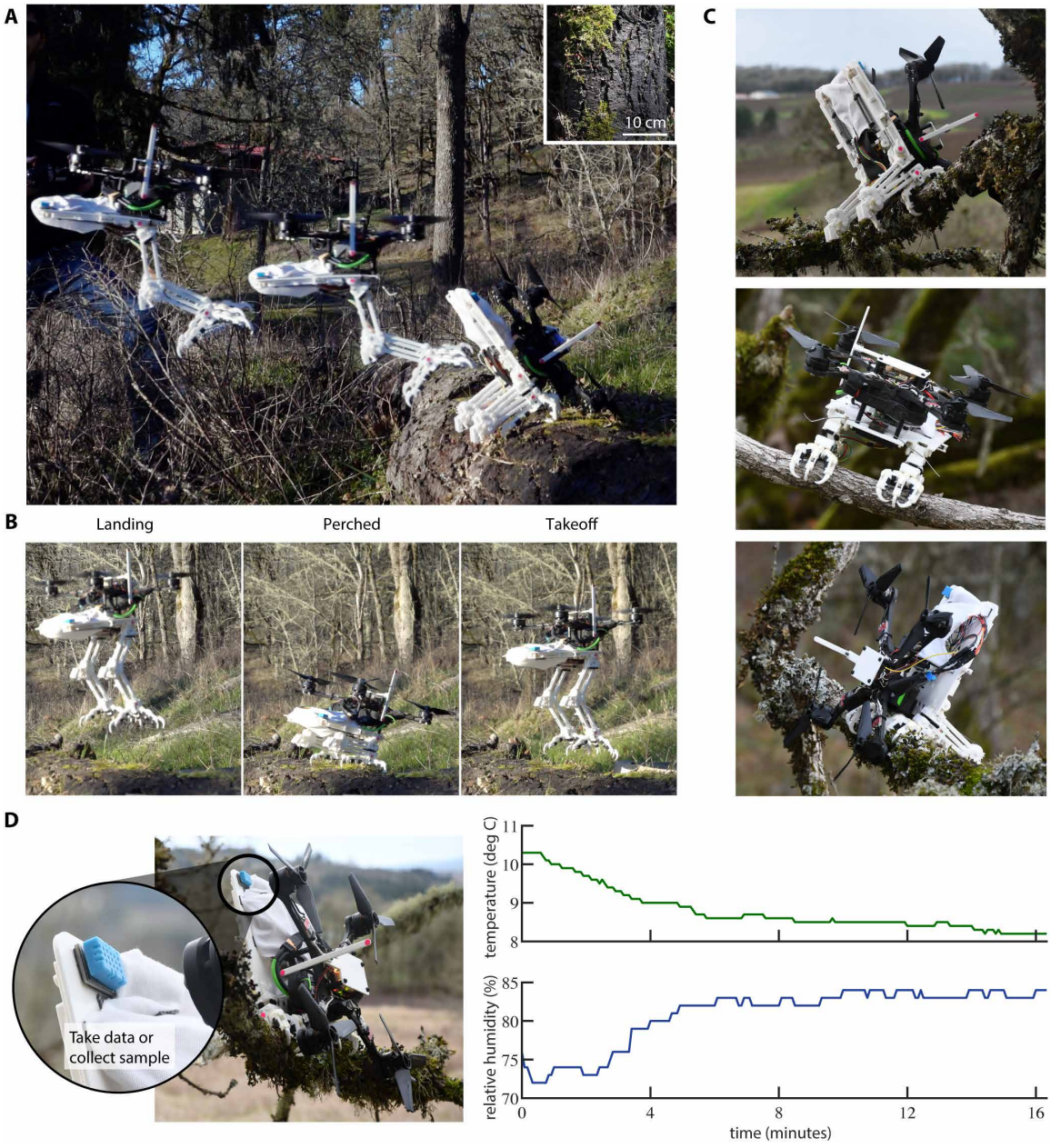


**Fig. 8. SNAG enables environmental monitoring in forests.** To demonstrate robustness in unstructured environments, we conducted tests in which SNAG landed on and took off from a tree branch in a forest in Oregon. (**A**) The composite image illustrates a robust near-horizontal landing despite high foot error during a dynamic bird-like approach. (**B**) The photos illustrate the landing, perching, and takeoff process (about 90 s between each photo) using a vertical approach typical for quadcopters and some specialized bird species (e.g., hummingbirds). The perch in (A) and (B) was from a fallen Douglas fir, which had a qualitatively similar texture to the large-diameter perch used in the indoor experiments shown in Fig. 6C (see inset, 242 mm in diameter). (**C**) Photos of SNAG perched on two different branches illustrate how SNAG can rest stably on branches of different sizes and orientations. For the purposes of the illustrative photos in (C) and (D), SNAG was placed by hand. (**D**) We illustrate how SNAG could be used to study ecosystems by measuring the ambient temperature and humidity onboard while perched [(A) to (D) data reported in data file S4).

to work in "real time" in complex environments, we need ways to interact with the world at higher speeds with sufficient accuracy even when there is limited information about the environment. To perch reliably, these robots should act to minimize the likelihood of leaving the perching sufficiency region because the value of every point in the space is equal or "good enough" for landing. More broadly, robots should act to minimize the likelihood of leaving the sufficiency region relevant to their goal.

Having outfitted SNAG with the two most common bird toe arrangements, zygodactyl (*58*), two toes in the front and two toes in the back similar to parrotlets, and anisodactyl (*56*), three toes in the front and one toe in the back similar to peregrine falcons (Fig. 4B),

we found only small differences in perching performance. This suggests that perching does not form an evolutionary selection pressure that can, by itself, explain arboreal avian toe diversity. The ability of birds with both toe arrangements to perch successfully on branches, like we tested here, corroborates this claim (*14*, *56*, *57*). Likewise, robots will be able to perch similarly with both toe arrangements. Further, we qualitatively observed that, for both dynamic perching and prey capture, birds must absorb energy with their legs, conform their feet to complex surface features, and produce high forces superfast to grasp reliably based on feed-forward control. Our experiments show that SNAG's system designed for perching can also reliably catch objects flying into its peregrine-inspired feet and release them again (text S3). Thus, the evolution of legs and feet that could be used for both dynamic perching and catching prey on the wing may have been relatively straightforward and is within reach for aerial robots.

Last, SNAG's fast grasp performance is enhanced by its small, lightweight toes that accelerate rapidly, inspired by peregrine falcons (fig. S1 and data file S7), which makes it broadly applicable in field robotics applications (text S10). Because the speed of passive leg collapse drives how quickly the toes wrap a surface, the grasp speed changes with impact speed. We measured grasp speeds of about 10 ms when catching, <20 ms when the quick release was manually triggered, and 30 to 50 ms when perching (text S4). SNAG's grasp is more than four times faster than previous high-speed grasping mechanisms such as the 96-ms closing time in (*31*). In contrast, SNAG's grasp is on par with much smaller birds such as parrotlets, who wrap their feet in 19 ± 7 ms when perching (*1*). SNAG's speed is also on par with raptors catching and striking prey at 10 to 30 ms (from contact to closure of the free foot in single-footed collisions) (*68*). Our isometric scaling analysis (data file S7) shows that larger robots harnessing SNAG's design paradigm will ultimately produce slower locomotory responses, and their angular momentum on landing will increase with the length to the fifth power ($l^5$). To accommodate these scaling effects, larger robots can select less aggressive kinematics to reduce the angular momentum that their feet must sustain to stay in the grasping sufficiency region. Overall, its bird-inspired design features make SNAG well suited for perching aerial and arboreal field robots as a mobile sensor package to perform environmental and biodiversity monitoring. SNAG's demonstrated perching performance on real branches in a forest environment shows its potential to unlock research in complex arboreal environments at low cost (text S10), such as the XPRIZE for monitoring rainforest ecosystems.

## MATERIALS AND METHODS

### Perching sufficiency region model

The perching sufficiency region is a high-dimensional space in which the robot lands successfully. Variables that influence the region include the surface conditions as well as the robot's dynamics, hardware, and behavior (Fig. 3A). Our model of the sufficiency region uses the conditions at contact to determine whether the robot will succeed. Variables such as the robot's hardware design or balance behavior, for example, change how the robot responds to different contact conditions, which, in turn, alters the sufficiency region. Specifically, our model discretizes the space and tests mathematically whether each combination of variables is within the bounds that determine whether the landing is successful (implemented in MATLAB; data file S4). The robot's mass was modeled with two point masses: one at the center of mass of the body (to model the body) and one at the projected location of the center of mass on the axis of the legs (to model the legs). The variables that our model explicitly incorporated are speed ($v$), velocity direction ($\theta_v$), leg angle ($\theta_{leg}$), and foot misalignment ($e_{foot}$) (Fig. 3A). All other variables were held constant. We assumed that motion occurs in the sagittal plane and the quadrotor is level when the leg first contacts the perch. We validated these assumptions in our experiments using the data logs from the Pixracer (data file S8). Other variables that affect the sufficiency region, such as balance behavior and foot design, were factored into the bounds of the region.

The boundaries that constrain the sufficiency region in the model are primarily based on momentum (Fig. 6, A and B). The momentum equations were calculated in MotionGenesis (data file S2). The equation for the angular momentum about the center of the perch on impact is given in the "Grasp parameter sufficiency region" section (data file S4). As the leg collapses, gravity also affects the angular momentum of the robot. To model the effect of gravity, we added to the true momentum an effective gravity momentum term, which is linearly scaled as a function of leg angle to be 0 when the robot lands vertically. The final decision boundary was then determined by an effective angular momentum, $H_{Lx,eff} = H_{Lx} + H_{Lx,grav}$. We found that, when the leg angle is 45°, $H_{Lx,grav} = 0.124$ (kg·m$^2$)/s place $H_{Lx,eff} = 0$ (kg·m$^2$)/s near the center of the allowable angular momentum window. The final term needed to fully define the upper and lower bound on the angular momentum is the width of the angular momentum window. We found that an angular momentum window width of 0.04 (kg·m$^2$)/s agreed well with our data (Fig. 6B).

The linear momentum of the robot into the perch is given by $p_{Ly} = v * m_{robot} * \cos(\theta_{leg} - \theta_v)$. Just as for the angular momentum, the gravity acts on the robot as the leg collapses. We modeled this influence by adding a linear momentum term equal to the projection of momentum that would be gained by falling vertically for the time the leg collapses on the axis of the leg. Specifically, $p_{Ly,grav} = m_{robot} * g * t_{collapse} * \sin(\theta_{leg})$. Overall, $p_{Ly,eff} = p_{Ly} + p_{Ly,grav}$. Upper and lower limits were set on the linear momentum; the linear momentum must be large enough to collapse the leg but small enough to avoid breaking the robot. In this model, we assumed that there is no rebound with higher impact velocities, because rebound is partly absorbed by locking the ankle. The lower threshold was set to be 1.4715 (kg·m$^2$)/s, similar to the linear momentum gained if the robot were to drop vertically onto the perch with no initial velocity, which was sufficient to collapse the leg. The upper threshold is set to be twice the lower threshold. We did not experimentally test this limit to avoid damaging the robot.

To model the foot misalignment, we assumed that the angular momentum threshold begins to decrease at some foot misalignment value until the foot misalignment is so large that the foot fails to grasp the perch. Therefore, we linearly scaled the angular momentum thresholds from their value at zero misalignment to their mean value. This scaling begins at a foot misalignment of 0.0325 m and ends at 0.0425 m, which we found from pilot tests to be reasonable approximations.

The final factor that limits the sufficiency region takes into account the range of motion of the leg. If the leg angle at impact is too small, then the robot reaches the limit of the balance angle when attempting to balance and the quadrotor structure can interfere

with the perch surface. Thus, we set a lower limit of $\theta_{leg} = 20°$, which we determined to be a suitable value from pilot tests.

### Design of the laboratory-based perching experiments

To study how different mechanism designs and impact parameters affect perching, we constructed a setup that could produce consistent collisions between the robot and a perch. The robot was mounted to a slide on a rail that mechanically constrained the robot to have only one degree of freedom until the slide mechanically triggered the robot to be released a few millimeters away from contact with the perch (Fig. 4A). The robot was propelled by an elastic band stretched to a recorded distance to precisely control the impact speed. The rail could be rotated to test different velocity directions and translated to test different impact angles. The impact speed was controlled by launching the robot with an elastic band. A Sony RX10 III camera filming at 119.88 frames/s (shutter speed: 1/320; ISO: 1000; F7.1, 2.4-4/8.8-220 Vario-Sonnar T* lens) captured a side view of the landing (data file S4). To facilitate data analysis, we placed 6-mm circular pink stickers on the robot's foot and hip as well as on a structure protruding from the robot's body that served as a scale bar in the image frame. Accelerations during the tests were logged with the Pixracer's inertial measurement unit (IMU). The Pixracer was controlled with a Spektrum DX6 RC. A solid model of the setup is available in data file S1. The ranges of variables tested were all selected to be in the realm of realistic values for birds. A detailed discussion on how the variable values were selected can be found in text S5.

The steps for each experimental trial were as follows. First, the robot was turned on and armed to begin logging IMU data and prepare the grasping mechanism for landing. Then, the camera was set to record. A switch on the RC was toggled in view of the camera to align IMU data with the camera frames. Last, the robot was launched at the perch. Landings were considered successful if they resulted in the robot statically positioned on the perch with the foot center above the horizontal. In the case of a failed landing, the robot was caught as it fell. If we noticed any slack in the tendons during the experiments, then we tuned the tendon tensioners to rebalance the leg stiffnesses. To release the surface and reset the mechanism, the experimenter used the RC to initiate the release behavior.

### Design of the laboratory-based catching experiments

The laboratory-based catching experiments were conducted in a manner similar to the laboratory-based perching experiments. However, rather than launching the robot at the perch, the objects were hand-launched at a variety of speeds (4.49 ± 0.40 m/s) at the robot, which was held fixed on the rail. The three objects used were a prey model, a bean bag (JMEXSUSS Corn Hole bags), and a tennis ball (data file S3).

### Design of the outdoor perching and catching experiments

The outdoor perching and catching experiments were conducted in a similar manner to the laboratory-based perching and catching experiments. However, rather than using a rail system to launch the robot, the robot was manually flown by a remote pilot with the RC. As the robot landed, the experimenter toggled a switch to cut the throttle and trigger an emergency motor cut. After a successful landing, the robot then recorded temperature and humidity data and was manually controlled to fly away. The flights all took place in Oregon, USA, in a temperate deciduous and northern coniferous forest. For the catching test shown in Fig. 1C, the robot was flown manually in the air and objects were hand-launched at the robot. This $n = 1$ proof-of-concept test was done with the SNAG version that preceded the final version used in the laboratory-based experiments.

### Data analysis

The Pixracer IMU data were analyzed in MATLAB, and the data illustrate that the robot was not moving substantially out of the side view plane when it made contact with perches (data files S4 and S8). The IMU data and camera frames were aligned by finding the frame at which an RC switch was toggled, accounting for 40- to 60-ms delays in the IMU data found in the pilot tests. For the laboratory-based perching tests, we used MATLAB to automatically track the dots on the body, the hip, and the foot (data file S4 and fig. S3). From these tracked points, we could determine the landing kinematics, including the contact speed, the velocity direction, and the leg angle. We measured the foot misalignment manually. For the outdoor perching tests, we tracked these points automatically with the DLTdv8 digitizing tool (*69*). For the catching tests, objects were tracked by hand using the DLTdv8 digitizing tool. All trajectories were filtered with Eiler's perfect smoother (*70*).

### Animals

The peregrine falcon cadavers were collected under U.S. Fish and Wildlife Service Migratory Bird and Eagle Scientific Collecting permit number MB26135-1 and California Department of Fish and Wildlife scientific collecting permit number SC-12951 with an American Peregrine Falcon Research Memorandum of Understanding. The cadavers were acquired via the California Department of Fish and Wildlife.

## SUPPLEMENTARY MATERIALS

www.science.org/doi/10.1126/scirobotics.abj7562
Texts S1 to S11
Figs. S1 to S3
Table S1
Data files S1 to S8
Movie S1
References (*72–86*)

## REFERENCES AND NOTES


1. W. R. T. Roderick, D. D. Chin, M. R. Cutkosky, D. Lentink, Birds land reliably on complex surfaces by adapting their foot-surface interactions upon contact. *eLife* **8**, e46415 (2019).
2. P. Provini, A. Abourachid, Whole-body 3D kinematics of bird take-off: Key role of the legs to propel the trunk. *Sci. Nat.* **105**, 12 (2018).
3. R. H. C. Bonser, A. P. Norman, J. M. V. Rayner, Does substrate quality influence take-off decisions in common starlings? *Funct. Ecol.* **13**, 102–105 (1999).
4. K. E. Crandell, A. F. Smith, O. L. Crino, B. W. Tobalske, Coping with compliance during take-off and landing in the diamond dove (*Geopelia cuneata*). *PLOS ONE* **13**, e0199662 (2018).
5. D. N. Lee, General Tau Theory: Evolution to date. *Perception* **38**, 837–850 (2009).
6. D. N. Lee, M. N. O. Davies, P. R. Green, F. R. Van Der Weel, Visual control of velocity of approach by pigeons when landing. *J. Exp. Biol.* **180**, 85–104 (1993).
7. P. M. Galton, J. D. Shepherd, Experimental analysis of perching in the European starling (*Sturnus vulgaris*: Passeriformes; Passeres), and the automatic perching mechanism of birds. *J. Exp. Zool. A Ecol. Genet. Physiol.* **317**, 205–215 (2012).
8. L. Einoder, A. M. M. Richardson, An ecomorphological study of the raptorial digital tendon locking mechanism. *Ibis* **148**, 515–525 (2006).
9. S. B. Backus, D. Sustaita, L. U. Odhner, A. M. Dollar, Mechanical analysis of avian feet: Multiarticular muscles in grasping and perching. *R. Soc. Open Sci.* **2**, 140350 (2015).
10. S. A. Kane, M. Zamani, Falcons pursue prey using visual motion cues: New perspectives from animal-borne cameras. *J. Exp. Biol.* **217**, 225–234 (2014).
11. C. H. Brighton, A. L. R. Thomas, G. K. Taylor, Terminal attack trajectories of peregrine falcons are described by the proportional navigation guidance law of missiles. *Proc. Natl. Acad. Sci. U.S.A.* **114**, 13495–13500 (2017).

12. R. Mills, H. Hildenbrandt, G. K. Taylor, C. K. Hemelrijk, Physics-based simulations of aerial attacks by peregrine falcons reveal that stooping at high speed maximizes catch success against agile prey. *PLOS Comput. Biol.* **14**, e1006044 (2018).
13. D. Sustaita, F. Hertel, In vivo bite and grip forces, morphology and prey-killing behavior of North American accipiters (Accipitridae) and falcons (Falconidae). *J. Exp. Biol.* **213**, 2617–2628 (2010).
14. J. F. Botelho, D. Smith-Paredes, D. Nuñez-Leon, S. Soto-Acuña, A. O. Vargas, The developmental origin of zygodactyl feet and its possible loss in the evolution of Passeriformes. *Proc. Biol. Sci.* **281**, 20140765 (2014).
15. W. R. T. Roderick, M. R. Cutkosky, D. Lentink, Touchdown to take-off: At the interface of flight and surface locomotion. *Interface Focus* **7**, 20160094 (2017).
16. C. E. Doyle, J. J. Bird, T. A. Isom, J. C. Kallman, D. F. Bareiss, D. J. Dunlop, R. J. King, J. J. Abbott, M. A. Minor, An avian-inspired passive mechanism for quadrotor perching. *IEEE ASME Trans. Mechatron.* **18**, 506–517 (2013).
17. P. M. Nadan, T. M. Anthony, D. M. Michael, J. B. Pflueger, M. S. Sethi, K. N. Shimazu, M. Tieu, C. L. Lee, A bird-inspired perching landing gear system. *J. Mech. Robot.* **11**, 061002 (2019).
18. P. M. Nadan, C. L. Lee, Computational design of a bird-inspired perching landing gear mechanism, in *Proceedings of the ASME 2018 International Mechanical Engineering Congress and Exposition*, Pittsburgh, Pennsylvania, USA, 9 to 15 November 2018, pp. 1–8.
19. W. Chi, K. H. Low, K. H. Hoon, J. Tang, T. H. Go, A bio-inspired adaptive perching mechanism for unmanned aerial vehicles. *J. Robot. Mechatron.* **24**, 642–648 (2012).
20. J. Thomas, J. Polin, K. Sreenath, V. Kumar, Avian-inspired grasping for quadrotor micro UAVs, in *Volume 6A: 37th Mechanisms and Robotics Conference* (American Society of Mechanical Engineers, 2013); http://proceedings.asmedigitalcollection.asme.org/proceeding.aspx?doi=10.1115/DETC2013-13289.
21. P. Yu, Z. Wang, K. C. Wong, Exploring aerial perching and grasping with dual symmetric manipulators and compliant end-effectors. *Int. J. Micro Air Veh.* **11**, 1–11 (2019).
22. H. Seo, S. Kim, H. J. Kim, Aerial grasping of cylindrical object using visual servoing based on stochastic model predictive control, in *Proceedings of the 2017 IEEE International Conference on Robotics and Automation (ICRA)*, Singapore, 29 May to 3 June 2017, pp. 6362–6368.
23. S. Kim, S. Choi, H. J. Kim, Aerial manipulation using a quadrotor with a two DOF robotic arm, in *Proceedings of the IEEE International Conference on Intelligent Robots and Systems*, Tokyo, Japan, 3 to 7 November 2013, pp. 4990–4995.
24. A. Gawel, M. Kamel, T. Novkovic, J. Widauer, D. Schindler, B. P. Von Altishofen, R. Siegwart, J. Nieto, Aerial picking and delivery of magnetic objects with MAVs, in *Proceedings of the 2017 IEEE International Conference on Robotics and Automation (ICRA)*, Singapore, 29 May to 3 June 2017, pp. 5746–5752.
25. S.-J. Kim, D.-Y. Lee, G.-P. Jung, K.-J. Cho, An origami-inspired, self-locking robotic arm that can be folded flat. *Sci. Robot.* **3**, eaar2915 (2018).
26. V. Ghadiok, J. Goldin, W. Ren, On the design and development of attitude stabilization, vision-based navigation, and aerial gripping for a low-cost quadrotor. *Auton. Robots.* **33**, 41–68 (2012).
27. S. Mishra, D. Yang, C. Thalman, P. Polygerinos, W. Zhang, Design and control of a hexacopter with soft grasper for autonomous object detection and grasping, in *Volume 3: Modeling and Validation; Multi-Agent and Networked Systems; Path Planning and Motion Control; Tracking Control Systems; Unmanned Aerial Vehicles (UAVs) and Application; Unmanned Ground and Aerial Vehicles; Vibration in Mechanical Systems; Vibrat* (American Society of Mechanical Engineers, 2018), pp. 1–9; https://asmedigitalcollection.asme.org/DSCC/proceedings/DSCC2018/51913/V003T36A003/270951.
28. X. Ding, P. Guo, K. Xu, Y. Yu, A review of aerial manipulation of small-scale rotorcraft unmanned robotic systems. *Chinese J. Aeronaut.* **32**, 200–214 (2019).
29. PRODRONE, Dual Robot Arm Large-Format Drone PD6B-AW-ARM, www.prodrone.com/products/pd6b-aw-arm/.
30. J. Fishman, S. Ubellacker, N. Hughes, L. Carlone, Dynamic grasping with a "soft" drone: From theory to practice. arXiv:2103.06465 [cs.RO] (11 March 2021).
31. A. McLaren, Z. Fitzgerald, G. Gao, M. Liarokapis, A passive closing, tendon driven, adaptive robot hand for ultra-fast, aerial grasping and perching, in *Proceedings of the IEEE/RSJ International Conference on Intelligent Robots and System (IROS)*, Macau, China, 3 to 8 Novermber 2019, pp. 5602–5607.
32. S. Kim, A. Shukla, A. Billard, Catching objects in flight. *IEEE Trans. Robot.* **30**, 1049–1065 (2014).
33. K. Hang, X. Lyu, H. Song, J. A. Stork, A. M. Dollar, D. Kragic, F. Zhang, Perching and resting—A paradigm for UAV maneuvering with modularized landing gears. *Sci. Robot.* **4**, eaau6637 (2019).
34. W. Chi, K. H. Low, K. H. Hoon, J. Tang, An optimized perching mechanism for autonomous perching with a quadrotor, in *Proceedings of the 2014 IEEE International Conference on Robotics and Automation*, Hong Kong, China, 31 May to 7 June 2014, pp. 3109–3115.
35. K. M. Popek, M. S. Johannes, K. C. Wolfe, R. A. Hegeman, J. M. Hatch, J. L. Moore, K. D. Katyal, B. Y. Yeh, R. J. Bamberger, Autonomous grasping robotic aerial system for perching (AGRASP), in *Proceedings of the IEEE/RSJ International Conference on Intelligent Robots and Systems (IROS)*, Madrid, Spain, 1 to 5 October 2018, pp. 6220–6225.
36. H. Zhang, J. Sun, J. Zhao, Compliant bistable gripper for aerial perching and grasping, in *Proceedings of the 2019 International Conference on Robotics and Automation (ICRA)*, Montreal, QC, Canada, 20 to 24 May 2019, pp. 1248–1253.
37. H.-N. Nguyen, R. Siddall, B. Stephens, A. Navarro-Rubio, M. Kovač, A passively adaptive microspine grapple for robust, controllable perching, in *Proceedings of the 2019 2nd IEEE International Conference on Soft Robotics (RoboSoft)*, Seoul, Korea (South), 14 to 18 April 2019, pp. 80–87.
38. C. Luo, L. Yu, P. Ren, A vision-aided approach to perching a bioinspired unmanned aerial vehicle. *IEEE Trans. Ind. Electron.* **65**, 3976–3984 (2018).
39. E. Culler, G. Thomas, C. Lee, A perching landing gear for a quadcopter, in *53rd AIAA/ASME/ASCE/AHS/ASC Structures, Structural Dynamics and Materials Conference* (AIAA, 2012), pp. 1–9; http://arc.aiaa.org/doi/abs/10.2514/6.2012-1722.
40. K. Zhang, P. Chermprayong, D. Tzoumanikas, W. Li, M. Grimm, M. Smentoch, S. Leutenegger, M. Kovac, Bioinspired design of a landing system with soft shock absorbers for autonomous aerial robots. *J. Field Robot.* **36**, 230–251 (2019).
41. T. H. Quinn, J. J. Baumel, The digital tendon locking mechanism of the avian foot (Aves). *Zoomorphology* **109**, 281–293 (1990).
42. B. M. Kilbourne, Scale effects and morphological diversification in hindlimb segment mass proportions in neognath birds. *Front. Zool.* **11**, 37 (2014).
43. M. B. Bennett, Allometry of the leg muscles of birds. *J. Zool.* **238**, 435–443 (1996).
44. A. B. Ward, P. D. Weigl, R. M. Conroy, Functional morphology of raptor hindlimbs: Implications for resource partitioning. *Auk* **119**, 1052–1063 (2002).
45. W. J. Bock, Experimental analysis of the avian passive perching mechanism. *Am. Zool.* **5**, 681 (1965).
46. N. Konow, E. Azizi, T. J. Roberts, Muscle power attenuation by tendon during energy dissipation. *Proc. R. Soc. B* **279**, 1108–1113 (2012).
47. E. Höfling, A. Abourachid, The skin of birds' feet: Morphological adaptations of the plantar surface. *J. Morphol.* **282**, 88–97 (2021).
48. M. Costa, thesis, Stanford University (2000).
49. L. U. Odhner, L. P. Jentoft, M. R. Claffee, N. Corson, Y. Tenzer, R. R. Ma, M. Buehler, R. Kohout, R. D. Howe, A. M. Dollar, A compliant, underactuated hand for robust manipulation. *Int. J. Rob. Res.* **33**, 736–752 (2014).
50. H. Stuart, S. Wang, O. Khatib, M. R. Cutkosky, The Ocean One hands: An adaptive design for robust marine manipulation. *Int. J. Rob. Res.* **36**, 150–166 (2017).
51. B. W. Tobalske, D. L. Altshuler, D. R. Powers, Take-off mechanics in hummingbirds (Trochilidae). *J. Exp. Biol.* **207**, 1345–1352 (2004).
52. P. R. Green, P. Cheng, Variation in kinematics and dynamics of the landing flights of pigeons on a novel perch. *J. Exp. Biol.* **201**, 3309–3316 (1998).
53. J. Thomas, M. Pope, G. Loianno, E. W. Hawkes, M. A. Estrada, H. Jiang, M. R. Cutkosky, V. Kumar, Aggressive flight with quadrotors for perching on inclined surfaces. *J. Mech. Robot.* **8**, 051007 (2016).
54. H. Jiang, M. T. Pope, E. W. Hawkes, D. L. Christensen, M. A. Estrada, A. Parlier, R. Tran, M. R. Cutkosky, in *Proceedings of the 2014 IEEE International Conference on Robotics and Automation (ICRA)*, Hong Kong, China, 31 May to 7 June 2014, pp. 3102–3108.
55. A. L. Desbiens, A. T. Asbeck, M. R. Cutkosky, Landing, perching and taking off from vertical surfaces. *Int. J. Rob. Res.* **30**, 355–370 (2011).
56. N. S. Proctor, P. J. Lynch, *Manual of Ornithology: Avian Structure & Function* (Yale Univ. Press, 1993).
57. W. J. Bock, W. D. Miller, The scansorial foot of the woodpeckers, with comments on the evolution of perching and climbing feet in birds. *Am. Mus. Novit.* 45 (1959).
58. W. J. Bock, Functional and evolutionary morphology of woodpeckers. *Ostrich* **70**, 23–31 (1999).
59. D. Sustaita, E. Pouydebat, A. Manzano, V. Abdala, F. Hertel, A. Herrel, Getting a grip on tetrapod grasping: Form, function, and evolution. *Biol. Rev.* **88**, 380–405 (2013).
60. R. N. Rosenfield, J. W. Schneider, J. M. Papp, W. S. Seegar, Prey of peregrine falcons breeding in West Greenland. *Condor* **97**, 763–770 (1995).
61. M. Hirose, K. Ogawa, Honda humanoid robots development. *Philos. Trans. A Math. Phys. Eng. Sci.* **365**, 11–19 (2007).
62. S. Collins, A. Ruina, R. Tedrake, M. Wisse, Efficient bipedal robots based on passive-dynamic walkers. *Science* **307**, 1082–1085 (2005).
63. K. A. Mazurek, B. J. Holinski, D. G. Everaert, R. B. Stein, R. Etienne-Cummings, V. K. Mushahwar, Feed forward and feedback control for over-ground locomotion in anaesthetized cats. *J. Neural Eng.* **9**, 026003 (2012).
64. B. Goller, P. S. Segre, K. M. Middleton, M. H. Dickinson, D. L. Altshuler, Visual sensory signals dominate tactile cues during docked feeding in hummingbirds. *Front. Neurosci.* **11**, 622 (2017).
65. R. Necker, Specializations in the lumbosacral vertebral canal and spinal cord of birds: Evidence of a function as a sense organ which is involved in the control of walking. *J. Comp. Physiol. A* **192**, 439–448 (2006).

66. C. Ferrari, J. Canny, Planning optimal grasps, in *Proceedings of the 1992 IEEE International Conference on Robotics and Automation*, Nice, France, 12 to 14 May 1992, pp. 2290–2295.
67. D. Morrison, P. Corke, J. Leitner, Learning robust, real-time, reactive robotic grasping. *Int. J. Rob. Res.* **39**, 183–201 (2020).
68. G. E. Goslow Jr., The attack and strike of some North American raptors. *Auk* **88**, 815–827 (1971).
69. T. L. Hedrick, Software techniques for two- and three-dimensional kinematic measurements of biological and biomimetic systems. *Bioinspir. Biomim.* **3**, 034001 (2008).
70. P. H. C. Eilers, A perfect smoother. *Anal. Chem.* **75**, 3631–3636 (2003).
71. G. E. Hudson, Studies on the muscles of the pelvic appendage in birds. *Am. Midl. Nat.* **18**, 1–108 (1937).
72. K. Dermitzakis, J. P. Carbajal, J. H. Marden, Scaling laws in robotics. *Procedia Comput. Sci.* **7**, 250–252 (2011).
73. P. Mitiguy, *Dynamics of Mechanical, Aerospace, and Biomechanical Systems* (Motion Genesis LLC, 2013).
74. S. B. Backus, L. U. Odhner, A. M. Dollar, Design of hands for aerial manipulation: Actuator number and routing for grasping and perching, in *2014 IEEE/RSJ International Conference on Intelligent Robots and Systems*, Chicago, IL, USA, 14 to 18 September 2014, pp. 34–40.
75. A. Zeffer, L. C. Johansson, Å. Marmebro, Functional correlation between habitat use and leg morphology in birds (*Aves*). *Biol. J. Linn. Soc.* **79**, 461–484 (2003).
76. A. Stoessel, B. M. Kilbourne, M. S. Fischer, Morphological integration versus ecological plasticity in the avian pelvic limb skeleton. *J. Morphol.* **274**, 483–495 (2013).
77. A. V. L. Pike, D. P. Maitland, Scaling of bird claws. *J. Zool.* **262**, 73–81 (2004).
78. L. R. Tsang, P. G. McDonald, A comparative study of avian pes morphotypes, and the functional implications of Australian raptor pedal flexibility. *Emu - Austral Ornithol.* **119**, 14–23 (2019).
79. NOVA, *World's Fastest Animal* (PBS, 2018); www.pbs.org/wgbh/nova/video/worlds-fastest-animal/.
80. M. Burrows, G. Sutton, Interacting gears synchronize propulsive leg movements in a jumping insect. *Science* **341**, 1254–1256 (2013).
81. D. D. Chin, D. Lentink, How birds direct impulse to minimize the energetic cost of foraging flight. *Sci. Adv.* **3**, e1603041 (2017).
82. P. Provini, B. W. Tobalske, K. E. Crandell, A. Abourachid, Transition from wing to leg forces during landing in birds. *J. Exp. Biol.* **217**, 2659–2666 (2014).
83. M. N. O. Davies, P. R. Green, Optic flow-field variables trigger landing in hawk but not in pigeons. *Naturwissenschaften* **77**, 142–144 (1990).
84. L. A. France, thesis, University of Oxford (2019).
85. T. Adão, J. Hruška, L. Pádua, J. Bessa, E. Peres, R. Morais, J. J. Sousa, Hyperspectral imaging: A review on UAV-based sensors, data processing and applications for agriculture and forestry. *Remote Sens.* **9**, 1110 (2017).
86. T. R. Rambo, M. P. North, Canopy microclimate response to pattern and density of thinning in a Sierra Nevada forest. *For. Ecol. Manage.* **257**, 435–442 (2009).


**Acknowledgments:** We would like to thank J. E. Low for assembling the aerial quadrotor platform used in this work and for contributing to early pilot tests. We would also like to thank E. Chang and E. Pelos for feedback on the robot design, experimental setups, and ideas in this manuscript. We would like to thank D. Chin for insight into how birds take off and land. Last, we are grateful to K. Rogers (CDFW) and C. Battistone (CDFW) for help with acquiring the peregrine falcon cadavers. **Funding:** This research was supported by AFOSR DESI award number FA9550-18-1-0525 with special thanks to B. L. Lee, F. A. Leve, and J. L. Cambier for leading the program. In addition, W.R.T.R. was supported by an NSF Graduate Research Fellowship (DGE-114747), and D.L. was supported by grant NSF CAREER Award 1552419.
**Author contributions:** W.R.T.R. designed and constructed the grasping mechanism. W.R.T.R. assembled the robot components. All authors contributed feedback on the robot and experimental setup design. W.R.T.R. conducted all data collection and data analysis. W.R.T.R. made the figures, and W.R.T.R and D.L. wrote the paper. All authors reviewed the paper and contributed feedback. D.L. and M.R.C. contributed advice and supervised the work.
**Competing interests:** The authors declare that they have no competing interests. **Data and materials availability:** All data needed to evaluate the conclusions in the paper are present in the paper or the Supplementary Materials.

Submitted 31 May 2021
Accepted 3 November 2021
Published 1 December 2021
10.1126/scirobotics.abj7562